Supporting Information

Activating $BaWO_4$ ceramic through the atomic-level Ni doping for enhanced hydrogen evolution reaction

Zhendian Li[a], Yuan Ha[a,b*], Ziqi An[a], Xian Cao[a], Linzhuang Xing[a], Zhimin Li[a*]

Z. Li, Y. Ha, Z. An, X. Cao, L. Xing, Z. Li

[a]School of Advanced Materials and Nanotechnology, Xidian University, Xi'an 710071, P. R. China

[b]Building B5, Guangzhou Institute of Technology, Xidian University, China-Singapore Guangzhou Knowledge City, Huangpu District, Guangzhou, China

*Corresponding author. E-mail: hayuan@xidian.edu.cn (Y. Ha), lizhmin@163.com (Z. Li)

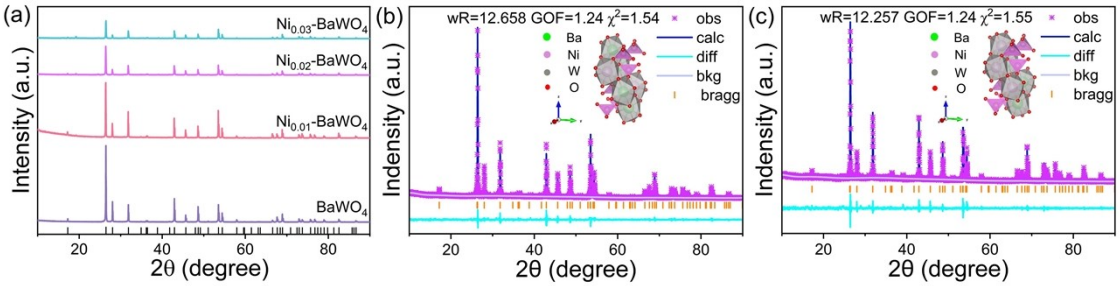

Figure S1. (a) XRD pattern of Ni_x-$BaWO_4$; (b) Rietveld refinement profile and crystal structure of pure $Ni_{0.02}$-$BaWO_4$ and (c) $Ni_{0.03}$-$BaWO_4$ ceramics.

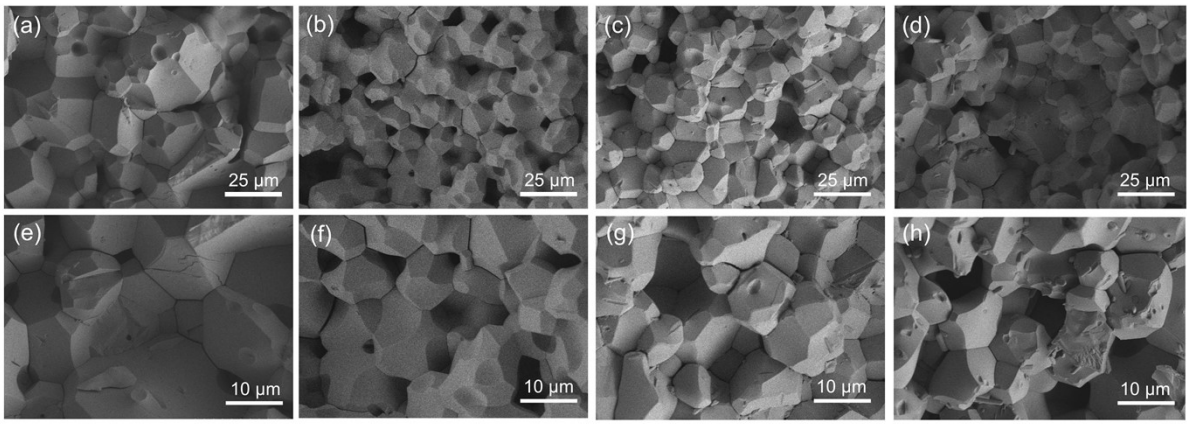

Figure S2. (a) and (e) SEM images of $BaWO_4$; (b) and (f) SEM images of $Ni_{0.01}$-$BaWO_4$; (c) and (g) SEM images of $Ni_{0.02}$-$BaWO_4$; (d) and (h) SEM images of $Ni_{0.03}$-$BaWO_4$.

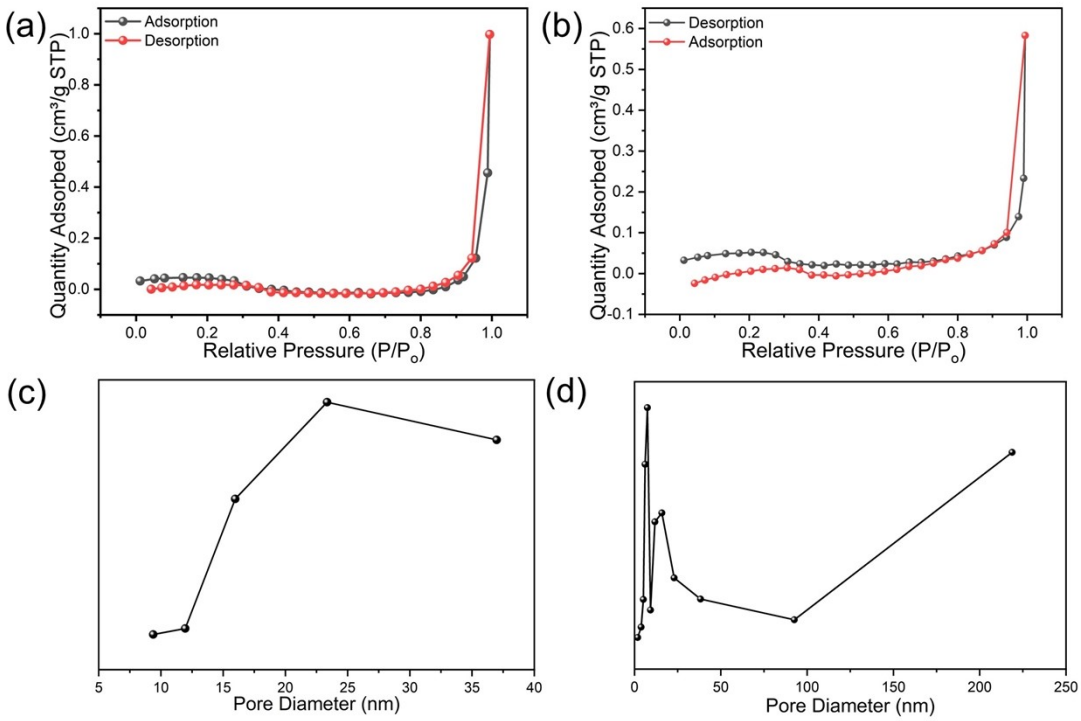

Figure S3. (a) The N_2 adsorption/desorption isotherm of $BaWO_4$ ceramics; (b) The N_2 adsorption/desorption isotherm of $Ni_{0.01}$-$BaWO_4$ ceramics; (c) The pore size distribution of $BaWO_4$ ceramics; (d) The pore size distribution of $Ni_{0.01}$-$BaWO_4$ ceramics.

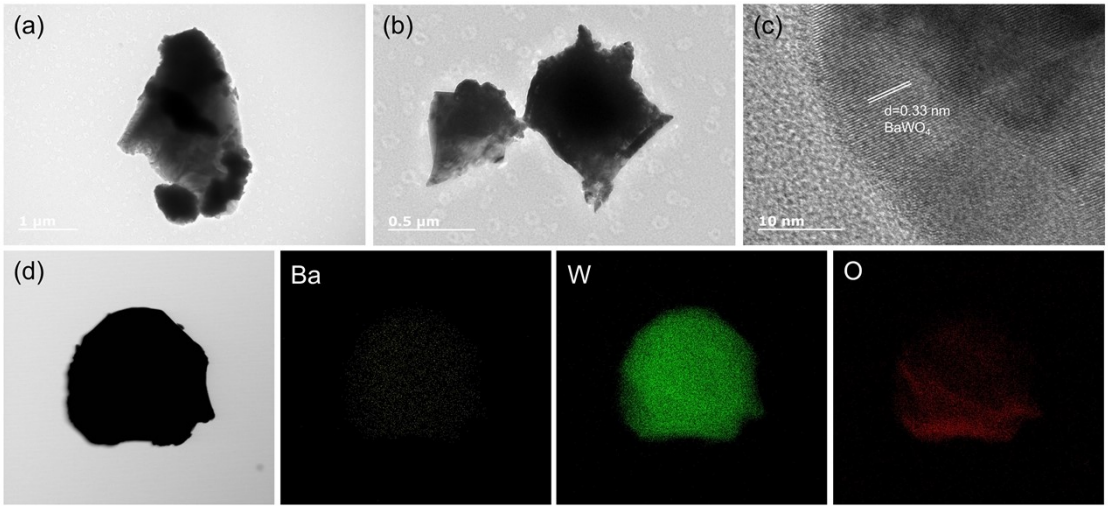

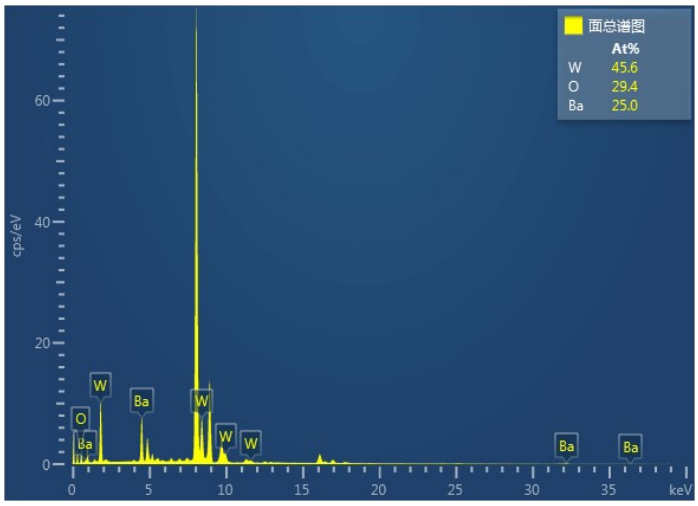

Figure S4. TEM and EDS mapping images of $BaWO_4$.

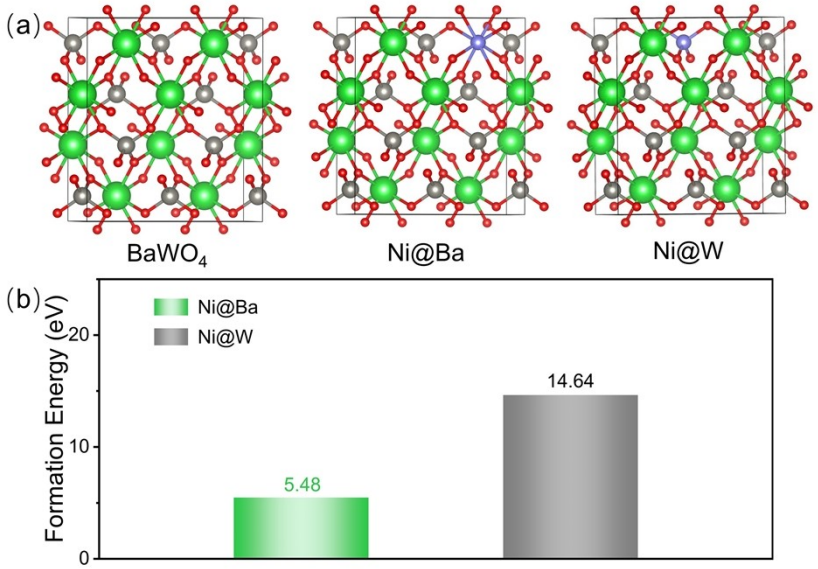

Figure S5. (a) Structural models of $BaWO_4$, Ni@Ba, and Ni@W; (b) Formation energies of Ni@Ba and Ni@W.

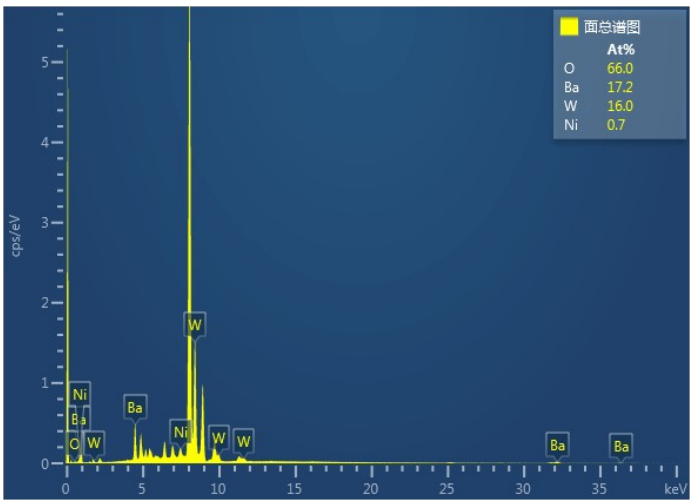

Figure S6. Elemental content distribution of EDS spectra of $Ni_{0.01}$-$BaWO_4$.

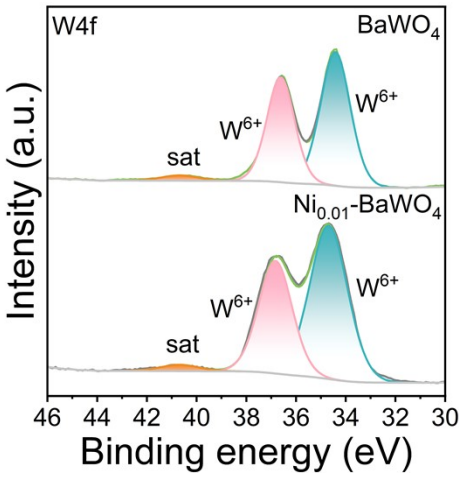

Figure S7. High-resolution W 4f XPS spectra of $BaWO_4$ and $Ni_{0.01}$-$BaWO_4$.

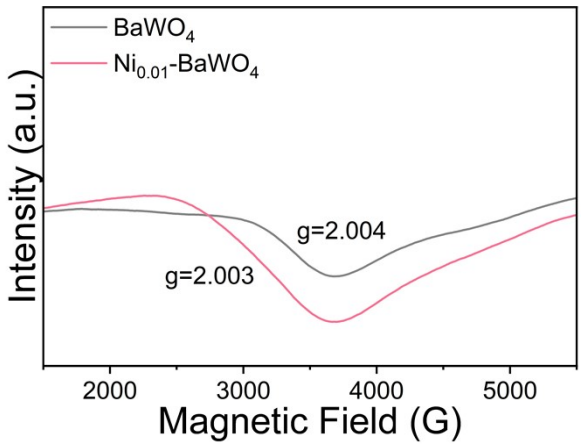

Figure S8. The EPR spectra of $BaWO_4$ and $Ni_{0.01}$-$BaWO_4$.

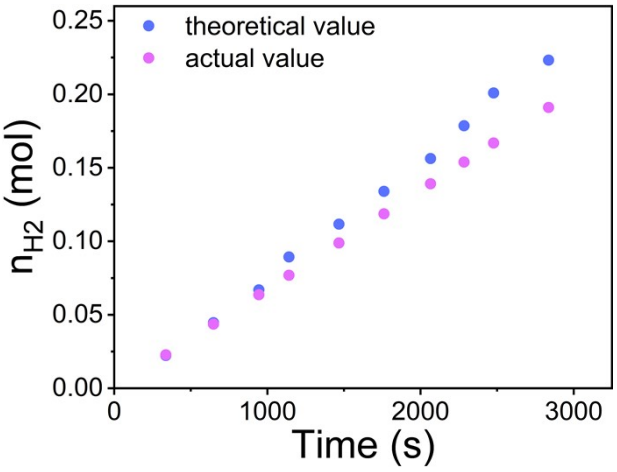

Figure S9. Graph of hydrogen production at different times.

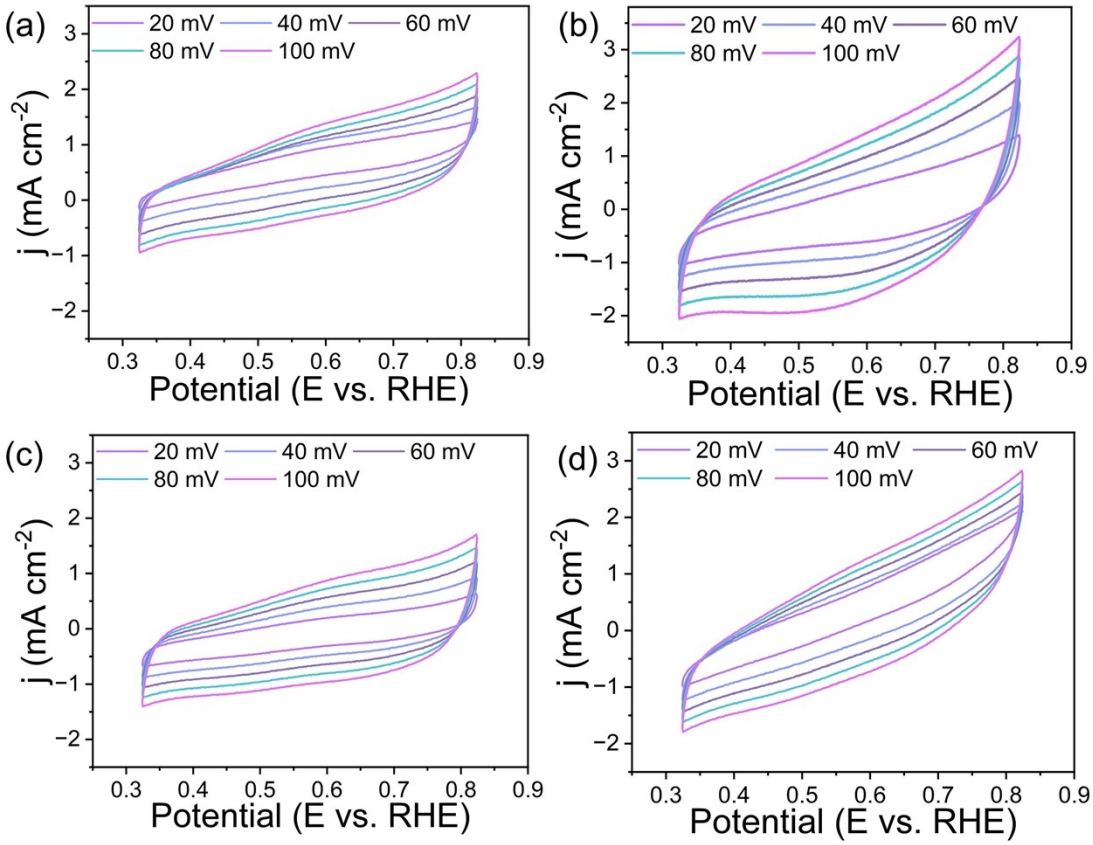

Figure S10. (a) $BaWO_4$; (b) $Ni_{0.01}$-$BaWO_4$; (c) $Ni_{0.02}$-$BaWO_4$; (d) $Ni_{0.03}$-$BaWO_4$;at different scan rates for CV

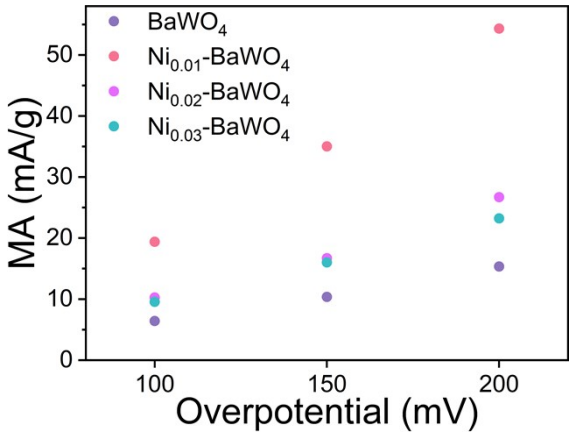

Figure S11. The mass activity of four catalyst.

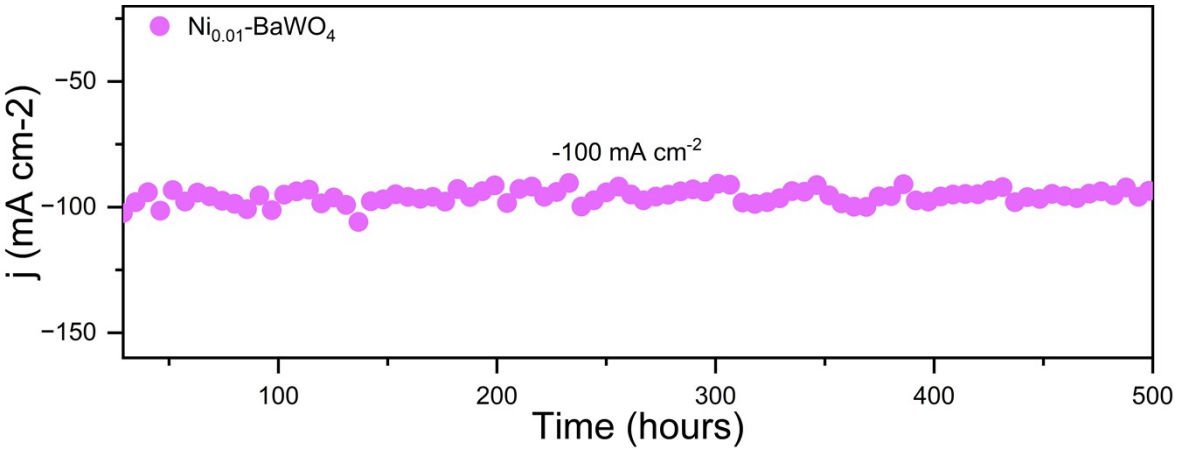

Figure S12. I-t curves of $Ni_{0.01}$-$BaWO_4$ at current densities of 100 mA cm^{-2}.

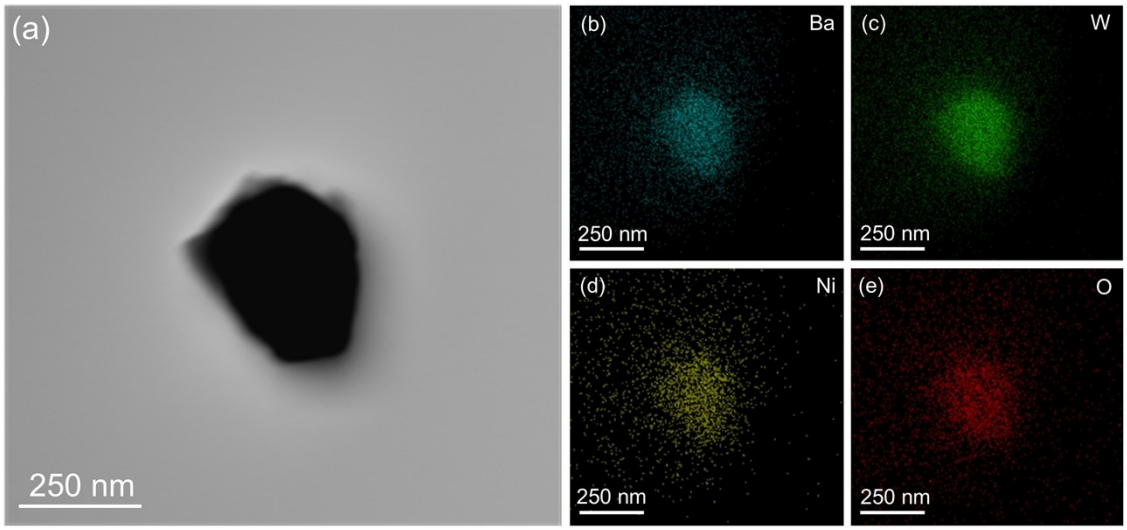

Figure S13. EDS mapping images of $Ni_{0.01}$-$BaWO_4$ after 500-hour long cycling.

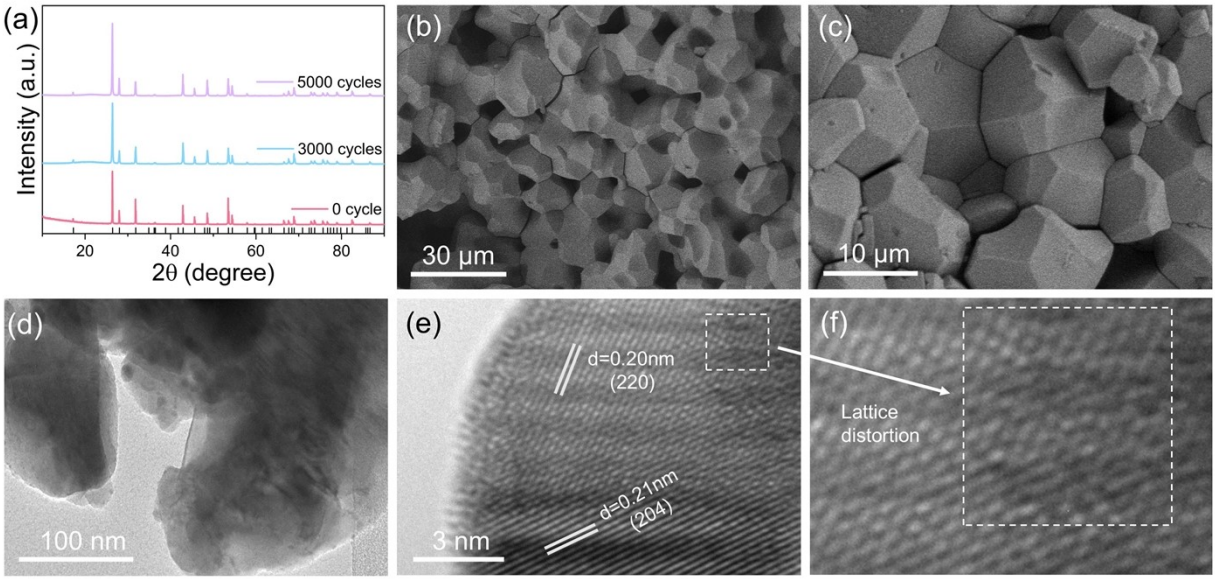

Figure S14. (a) At the current density of 100 mA cm^{-2}, $Ni_{0.01}$-$BaWO_4$ was XRD before and after the long-term cycle; (b-c) SEM images of $Ni_{0.01}$-$BaWO_4$ at various magnifications; (d) TEM image of $Ni_{0.01}$-$BaWO_4$; (e-f) HRTEM images of $Ni_{0.01}$-$BaWO_4$

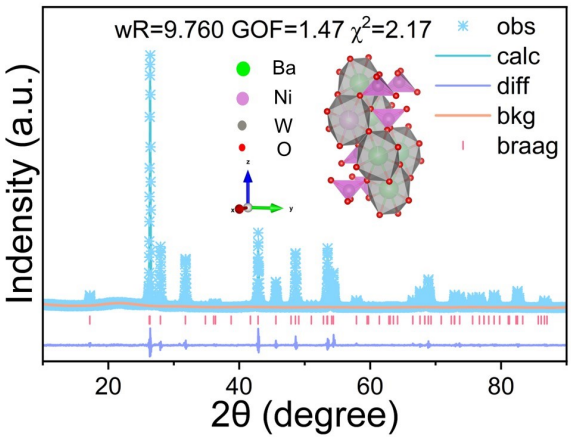

Figure S15. Rietveld refinement of $Ni_{0.01}$-$BaWO_4$ after 5000 cycles long-term cycling test.

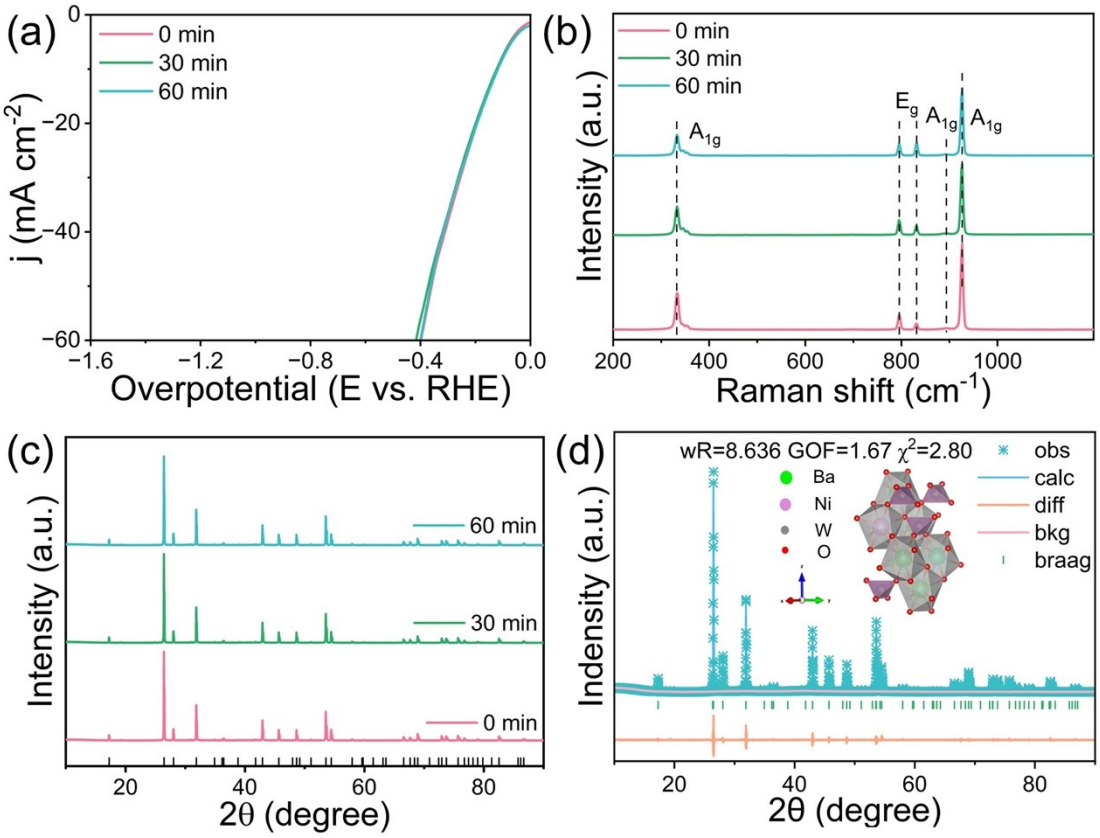

Figure S16. (a) HER polarization curves of $Ni_{0.01}$-$BaWO_4$ with different ultrasonication durations; (b) Raman spectra of $Ni_{0.01}$-$BaWO_4$ with different ultrasonication durations; (c) XRD of $Ni_{0.01}$-$BaWO_4$ after different ultrasonic time; (d) Rietveld refinement of $Ni_{0.01}$-$BaWO_4$ after 60 min ultrasonication.

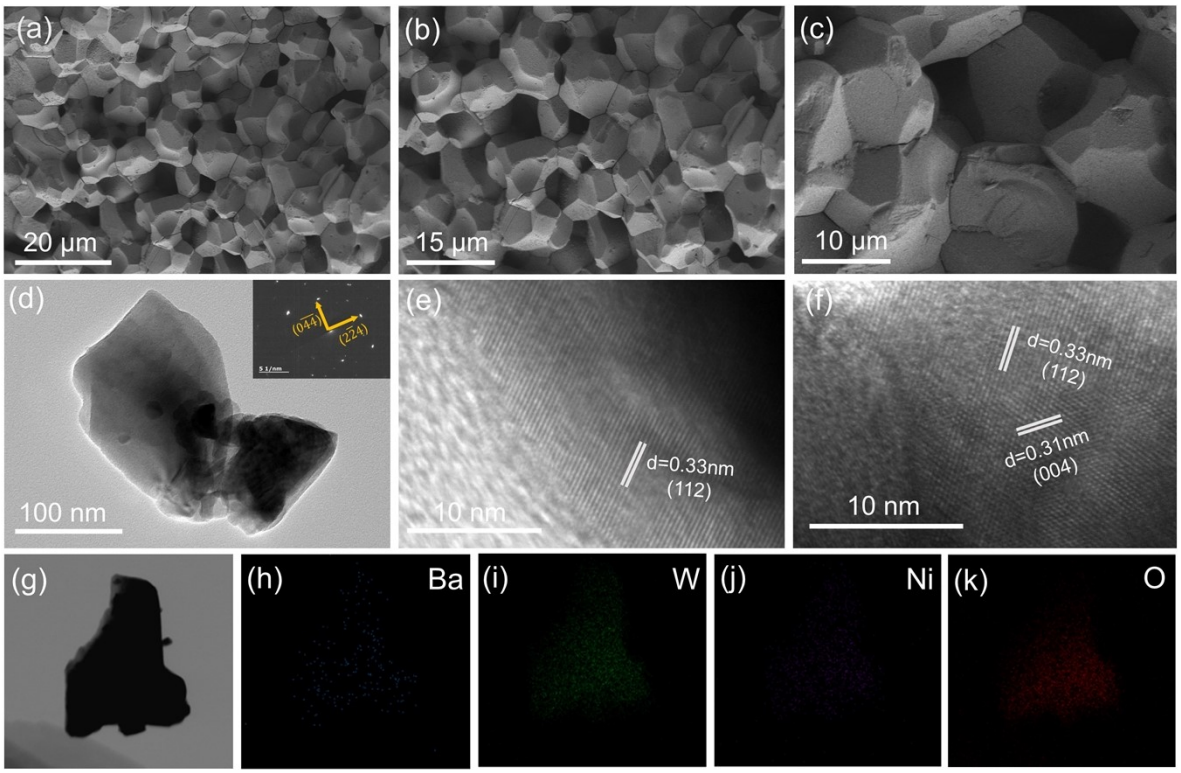

Figure S17. (a-c) SEM micrographs of $Ni_{0.01}$-$BaWO_4$ post 60 min sonication;(d) TEM image of $Ni_{0.01}$-$BaWO_4$ subjected to 60 min ultrasonic processing;(e-f) HRTEM images of $Ni_{0.01}$-$BaWO_4$ after 60 min ultrasonic;(g) STEM image of $Ni_{0.01}$-$BaWO_4$ following 60 min ultrasonic;(h-k) EDS elemental mapping images of $Ni_{0.01}$-$BaWO_4$ under 60 min ultrasonic.

Figure S18. EDS spectral element content distribution of $Ni_{0.01}$-$BaWO_4$ after ultrasound for 60 min.

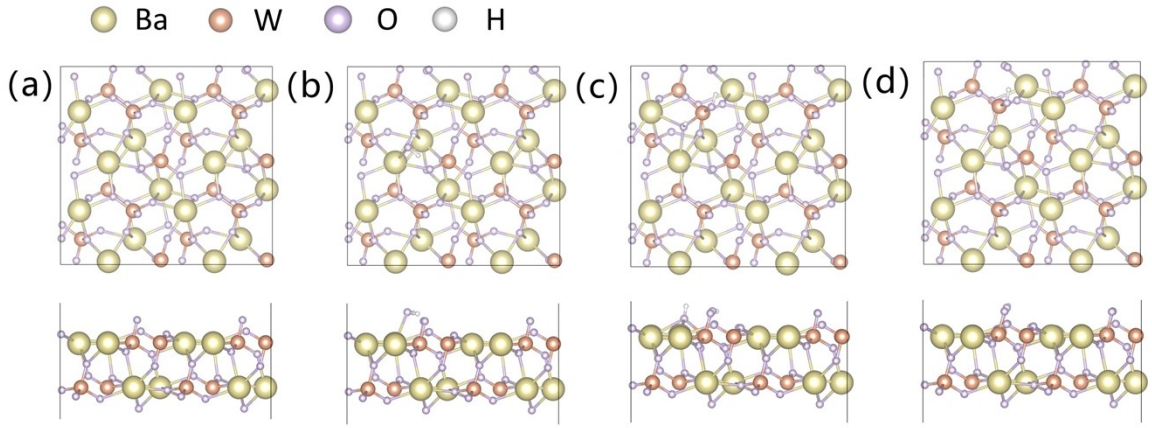

Figure S19. The adsorption model of $BaWO_4$ after structural optimizatio

Figure S20. The adsorption model of Ni-$BaWO_4$ after structural optimization.

Table S1 The porosity data of $BaWO_4$ and $Ni_{0.01}$-$BaWO_4$.

Samples	**Sample quality（g）**	**mercury intrusion volume（m_l/g）**	**Porosity （%）**
$BaWO_4$	1.6932	0.0286	14.7784
$Ni_{0.01}$-$BaWO_4$	1.6229	0.0424	20.6891

Table S2 The sintering density data of each sample.

Samples	m_1 for dry weight (g)	m_2 for buoyant weight (g)	m_3 for wet weight (g)	volume density (g cm^{-3})
$BaWO_4$	0.5512	0.5602	0.4606	5.534
$Ni_{0.01}$-$BaWO_4$	0.5516	0.5527	0.4494	5.340
$Ni_{0.02}$-$BaWO_4$	0.5539	0.5616	0.4595	5.425
$Ni_{0.03}$-$BaWO_4$	0.5534	0.5614	0.4602	5.468

Table S3. The BET data of $BaWO_4$ and $Ni_{0.01}$-$BaWO_4$.

Sample	Surface Area (m^2/g)	Pore Size (nm)
$BaWO_4$	0.1763	34.7529
$Ni_{0.01}$-$BaWO_4$	0.1963	29.2948

Table S4. The free energies of different samples.

	$BaWO_4$	Ni@Ba	Ni@W
Free energy (eV)	-350.07912	-344.59922	-335.43839

Table S5. ICP results of Ni_x-$BaWO_4$

Sample name	Sample quality m_0 (g)	Test element	Sample element content W (%)
$BaWO_4$	0.0446	Ba	44.85%
		W	55.12%
$Ni_{0.01}$-$BaWO_4$	0.0463	Ba	43.71%
		W	56.09%
		Ni	0.1%
$Ni_{0.02}$-$BaWO_4$	0.0428	Ba	38.85%
		W	57.85%
		Ni	0.22%
$Ni_{0.03}$-$BaWO_4$	0.0472	Ba	34.56%
		W	58.92%
		Ni	0.31%

Table S6. The EIS calculation parameters of the Ni_x-$BaWO_4$ sample were determined when performing HER in a 1 M KOH solution.

Samples	Rs (Ω)	Error(%)	Rct (Ω)	Error(%)	CPE	Error(%)
$BaWO_4$	29.45	1.0722	103.8	3.1642	0.5856	2.0774
$Ni_{0.01}$-$BaWO_4$	33.42	0.81424	31.41	3.1859	0.02	3.5134
$Ni_{0.02}$-$BaWO_4$	39.53	1.875	50.94	3.3092	0.5107	3.6752
$Ni_{0.03}$-$BaWO_4$	26.52	0.76459	57.21	1.2226	0.57799	1.3851

Table S7. Comparison of properties of $Ni_{0.01}$-$BaWO_4$ and other HER catalysts in alkaline solution

Catalyst	Electorlyte	Current density (j)	Overpotential	substrate	Ref.
$Ni_{0.01}$-$BaWO_4$	1 M KOH	10 mA cm^{-2}	122 mV	self-supporting	Our work
$BaBi_{1.9}Y_{0.1}Nb_2O_9$	1 M KOH	10 mA cm^{-2}	180 mV	NF	[1]
Mo_2C	1 M KOH	10 mA cm^{-2}	453 mV	self-supporting	[2]
P/Ni-Mo_2C@NC-800	1 M KOH	10 mA cm^{-2}	165 mV	NC	[3]
TiN	1 M KOH	10 mA cm^{-2}	483 mV	self-supporting	[4]
O-SiBCN/rGO	0.5 M H_2SO_4	10 mA cm^{-2}	590 mV	GC	[5]
PWA-2-1300	0.5 M H_2SO_4	10 mA cm^{-2}	286 mV	GC	[6]
$MoSi_2$	0.5 M H_2SO_4	10 mA cm^{-2}	241 mV	self-supporting	[7]
SiCN/Ni	0.5 M H_2SO_4	10 mA cm^{-2}	390 mV	CP	[8]
WS_2/WO_{3-x}	1 M KOH	10 mA cm^{-2}	151 mV	CP	[9]
a-WO_x	1 M KOH	10 mA cm^{-2}	185 mV	CC	[10]

Table S8. ICP test results of $Ni_{0.01}$-$BaWO_4$ after 500 hours of long-term use.

Sample name	m_0 (g)	Test element	Sample element content W (%)
Pristine $Ni_{0.01}$-$BaWO_4$	0.0453	Ni	0.1400%
$Ni_{0.01}$-$BaWO_4$ after 500 hours	0.0453	Ni	0.1393%
$Ni_{0.01}$-$BaWO_4$ after 500 hours	0.0453	Ni	0.1392%

Table S9. Rietveld refinement data of $Ni_{0.01}$-$BaWO_4$ after 5000 cycles long-term cycling test.

Sample	a axial length (Å)	b axial length (Å)	c axial length (Å)	Volume(Å^3)
$Ni_{0.01}$-BaWO4	5.612	5.612	12.713	400.343

Table S10. Rietveld refinement data of $Ni_{0.01}$-$BaWO_4$ after 60 min of ultrasonic vibration.

Sample	a axial length (Å)	b axial length (Å)	c axial length (Å)	Volume(Å^3)
$Ni_{0.01}$-$BaWO_4$	5.613	5.613	12.718	400.671

References

[1] M.K. Adak, D. Mondal, R. Samanta, B. Chakraborty and D. Dhak, *Ceram Int,* 2023, **49**, 1020.

[2] L. Huo, B. Liu, G. Zhang and J. Zhang, *ACS Appl. Mater. Interfaces,* 2016, **8**, 18107-18118.

[3] Z. Li, S. Xu, K. Chu, G. Yao, Y. Xu, P. Niu, Y. Yang and F. Zheng, *Inorg. Chem.,* 2020, **59**, 13741-13748.

[4] C. Tan, H. Huang, F. Wang, N. Ke, A. Huang, W. Tang, L. Hao, L. Yin, X. Xu, Y. Xian and S. Agathopoulos, *J Power Sources,* 2024, **610**, 234722.

[5] Q. Hanniet, M. Boussmen, J. Barés, V. Huon, I. Iatsunskyi, E. Coy, M. Bechelany, C. Gervais, D. Voiry, P. Miele and C. Salameh*, Sci. Rep.,* 2020,**10**, 22003.

[6] Z. Yu, K. Mao and Y. Feng, *J Adv Ceram,* 2021, **10**, 1338-1349.

[7] N. Ke, H. Huang, F. Wang, A. Huang, C. Tan, B. Dong, Y. Wu, L. Hao, X. Xu and S. Agathopoulos, *ACS Sustainable Chem. Eng.,* 2023, **11**, 3769-3779

[8] T.-H. Huh, J.H. Jun, J.-H. Lee, S. Moon, Y. Yoon, T. Lim, B.H. Kim and Y.-J. Kwark, *ACS Appl. Energy Mater.,* 2024, **7**, 10397-10406.

[9] L. Kong, L. Pan, H. Guo, Y. Qiu, W.A. Alshahrani, M.A. Amin and J. Lin, *J Colloid Interf Sci,* 2024, **664**, 178-185.

[10] J. Chen, J. Zheng, W. He, H. Liang, Y. Li, H. Cui and C. Wang, *Nano Res* 2023, **16**, 4603-4611.